Plasma transport across high latitudes

Dimitry Pokhotelov, Isabel Fernandez-Gomez, Florian Günzkofer,
and Claudia Borries

Institute for Solar-Terrestrial Physics (SO-SKP),
German Aerospace Centre (DLR), Neustrelitz, Germany

EGU General Assembly
Vienna, 26-May-2022

DLR

Earth's Magnetosphere

- Magnetosphere is the region of space where the Earth's own magnetic field dominates.
- Under southward IMF conditions, the merging of magnetic field lines is possible at the nose of magnetosphere (dayside reconnection).
- Closed magnetic field lines have both ends linked to the Earth; open field lines have one end linked to the solar wind.

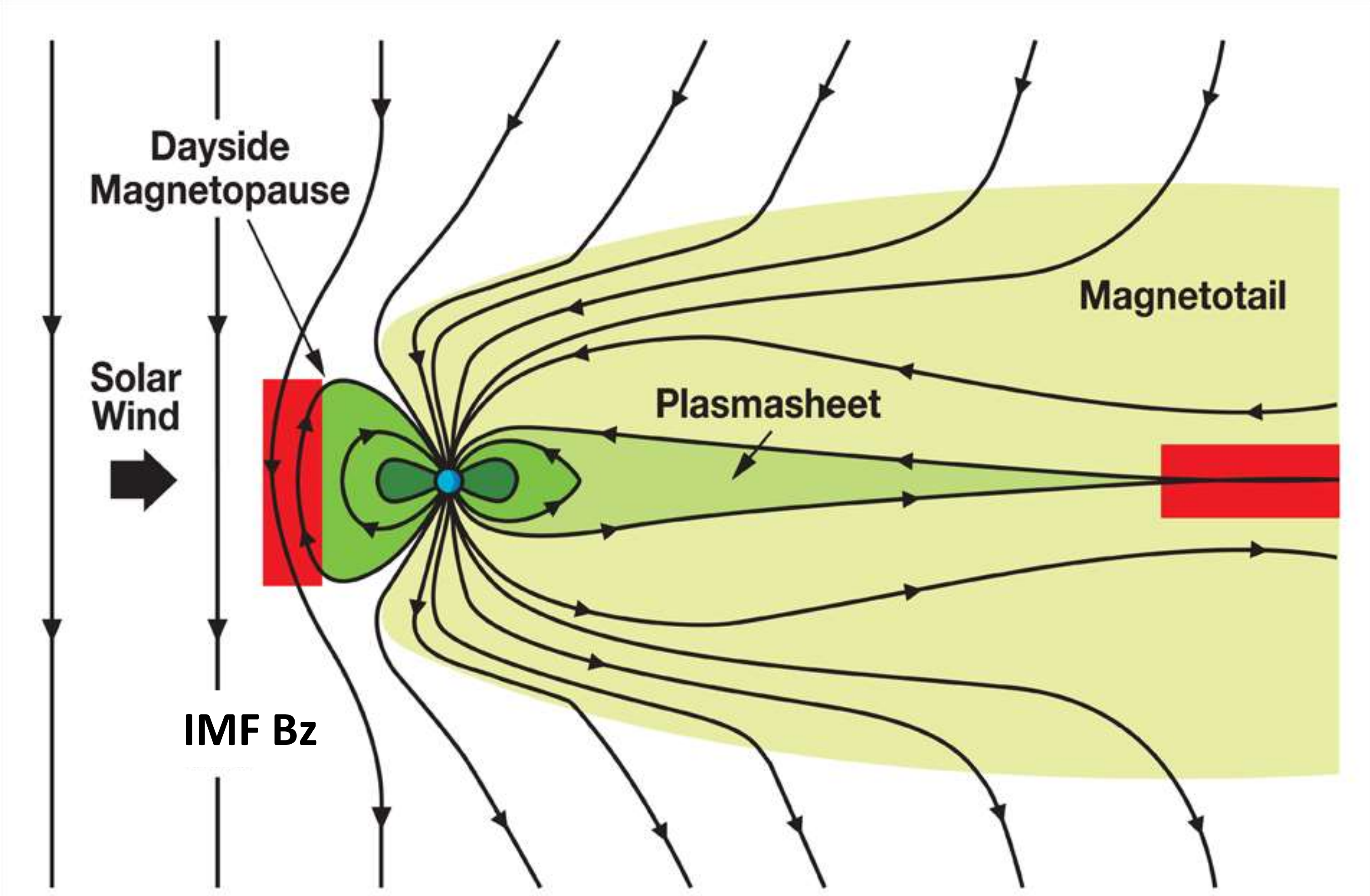

Courtesy of NASA

Coupling under southward IMF

Solar wind electric field (frozen-in plasma)

$$\mathbf{E}_{\mathrm{sw}} = -\mathbf{V}_{\mathrm{sw}} \times \mathbf{B}_{\mathrm{sw}}$$

Under a southward IMF, a dawn-to-dusk solar wind electric field $\mathbf{E}_{sw}$ maps to the polar cap ionosphere.

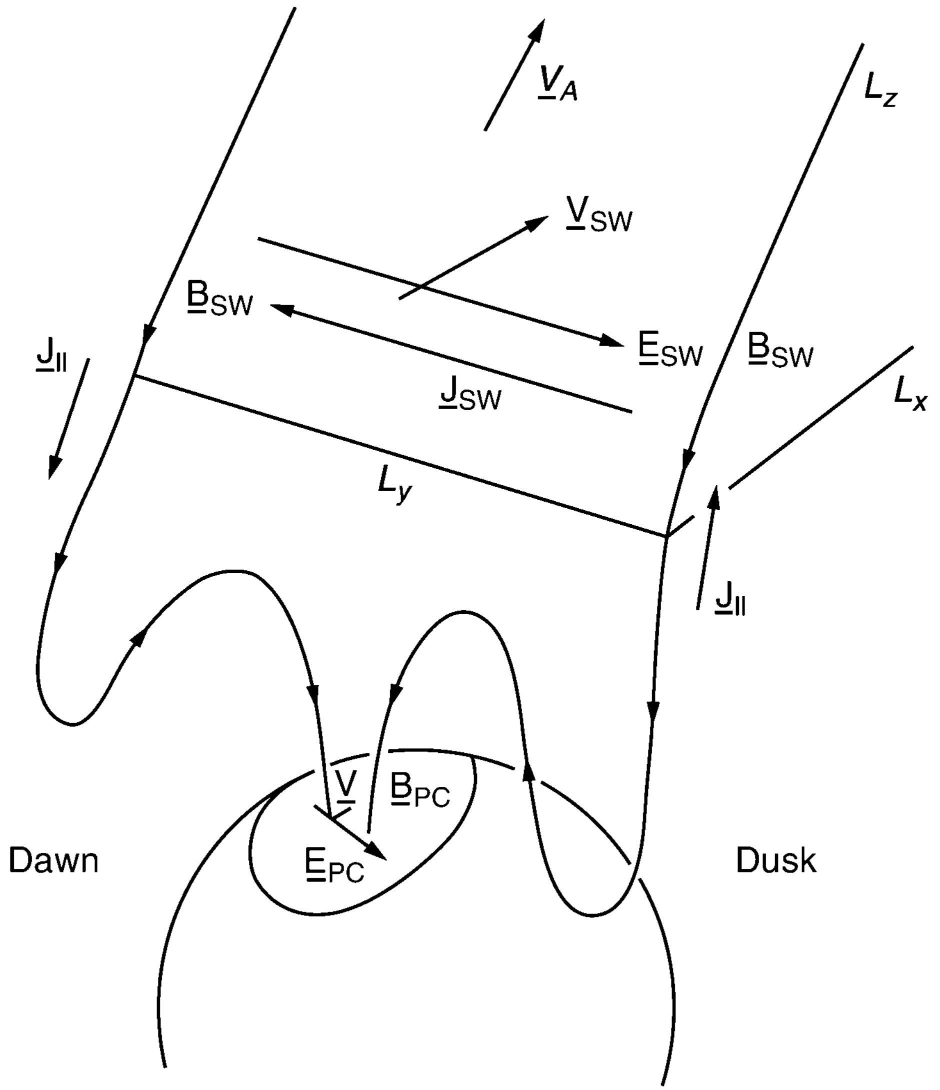

Satellite navigation systems

GPS system

~ 30 navigational GPS spacecraft

55° inclination orbits

Broadcast two frequencies in L1 and

L2 bands (1.57 and 1.23 GHz).

Other similar GNSS systems:

GLONASS, Galileo, Beidou

Ionosphere is a dispersive media

Total electron content (TEC) along the signal path from GPS spacecraft to the receiver can be inferred by measuring the phase advance and/or the group delay between different frequencies.

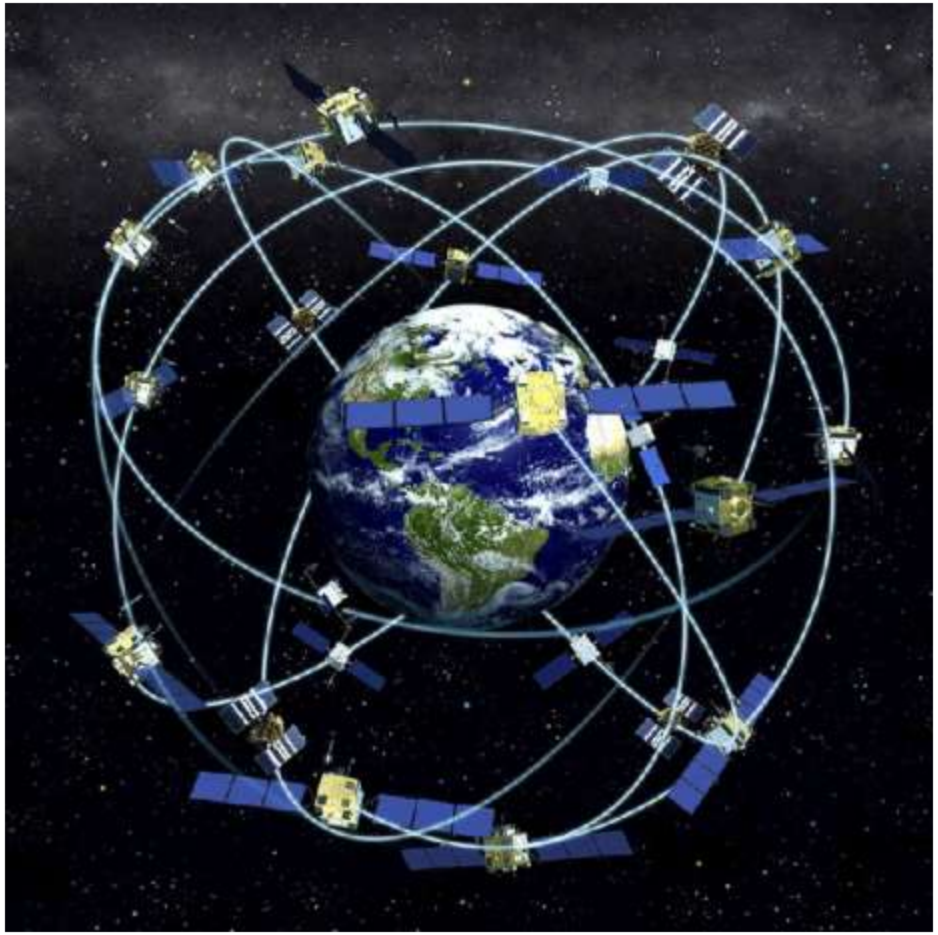

GNSS tomography example-1

Network of ground dual-frequency GNSS receivers at high latitudes.

Tomographic inversion of the GNSS data should reveal plasma dynamics.

Network of GNSS receivers

Projection of the tomographic grid

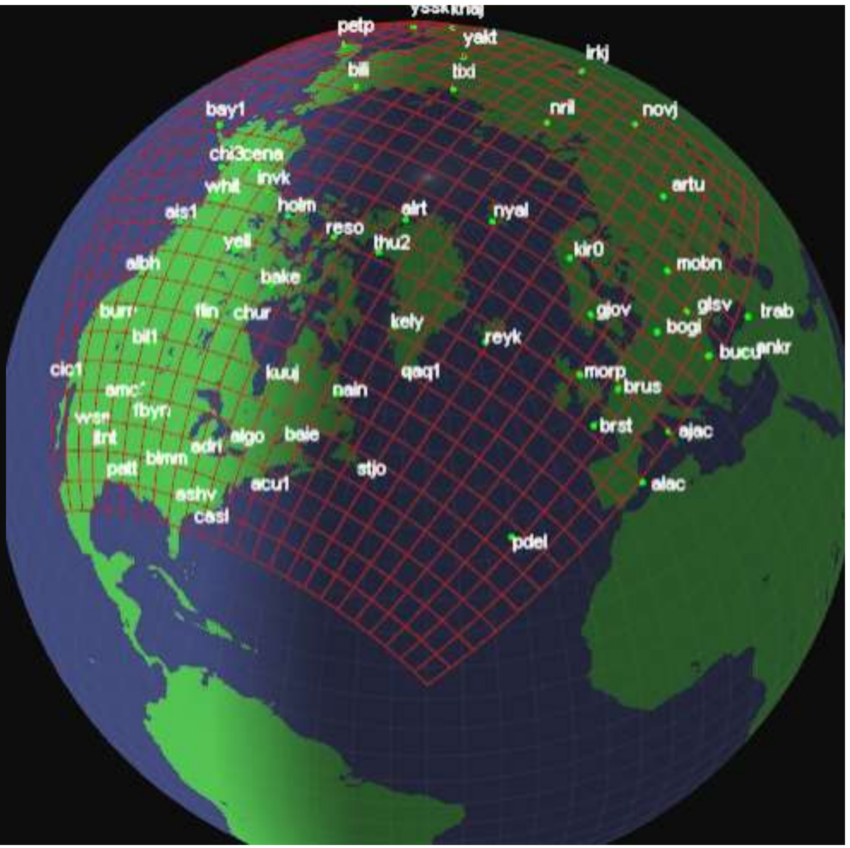

DLR

GNSS tomography example-2

Rays of GPS signals received during the major 30-Oct-2003 geomagnetic storm.

Colour shows plasma content along the ray.

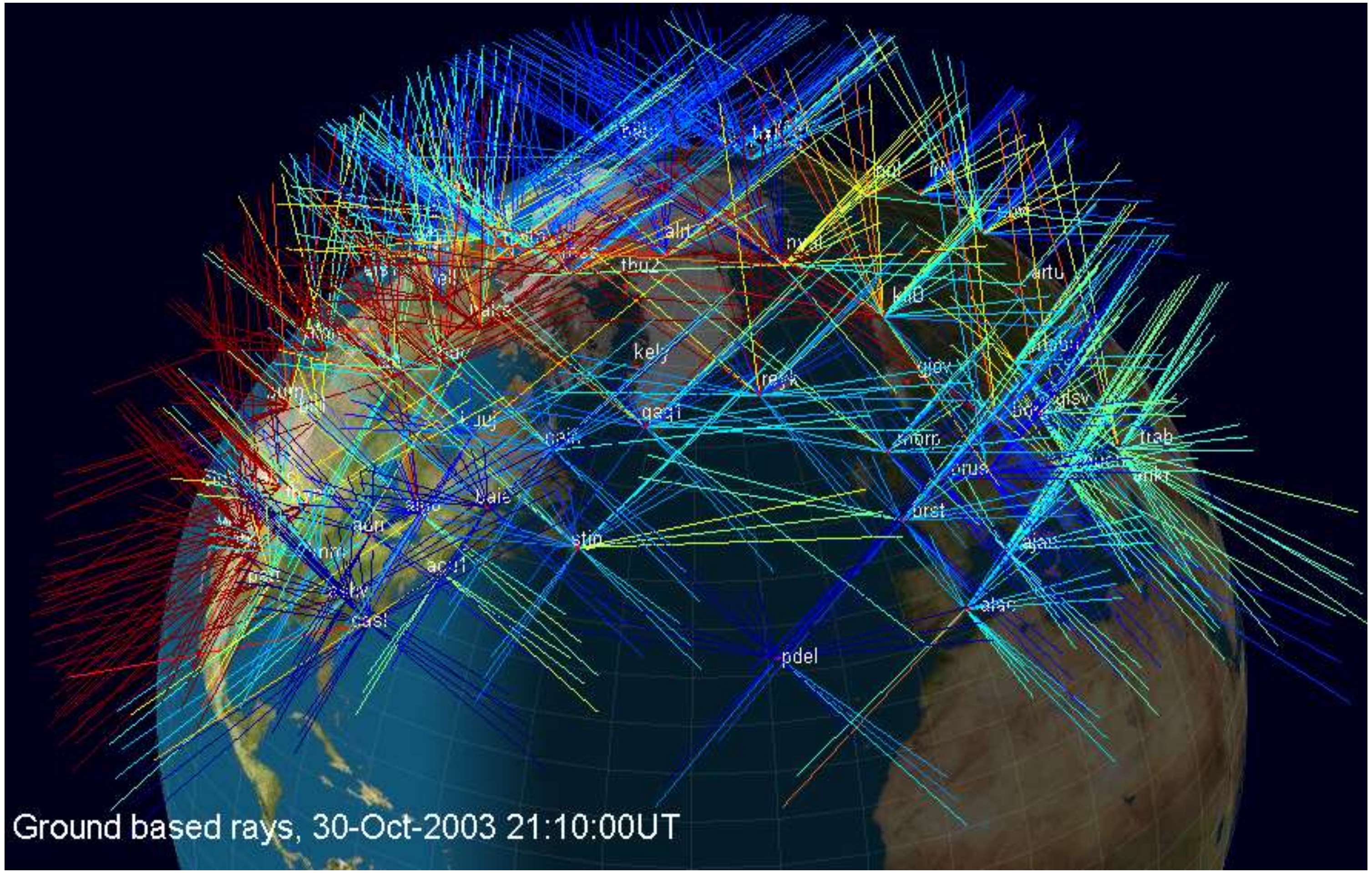

GNSS tomography example-3

Results of the tomographic reconstruction: plasma density

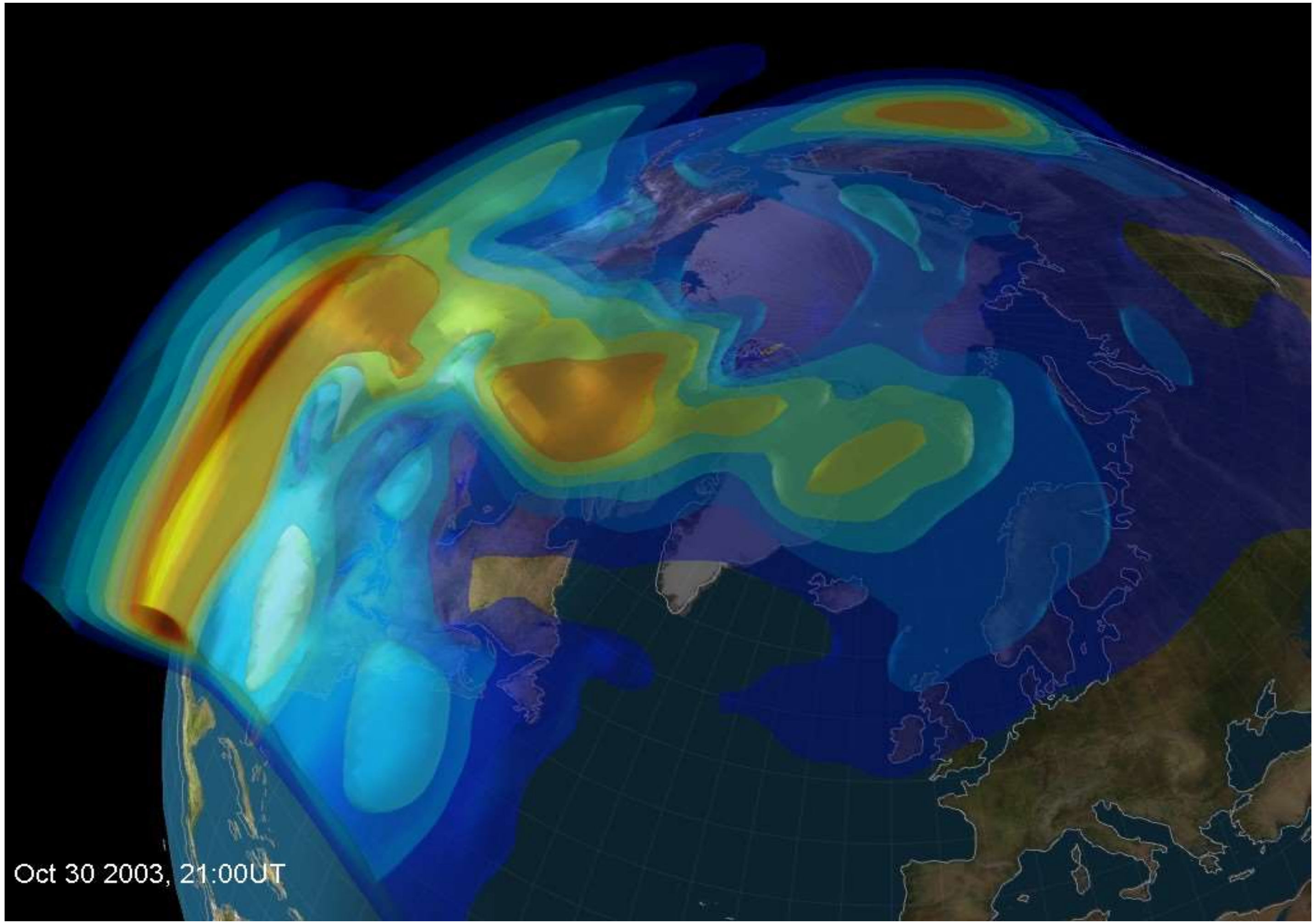

The global distribution of ionospheric plasma density can be deduced from characteristics of GPS signals acquired by ground-based network of GPS receivers.

Plasma follows general anti-sunward cross-polar convection.

DLR

Comparison with ground radar observations

Electron density during 30-Oct-2003 storm as a function of height and UT

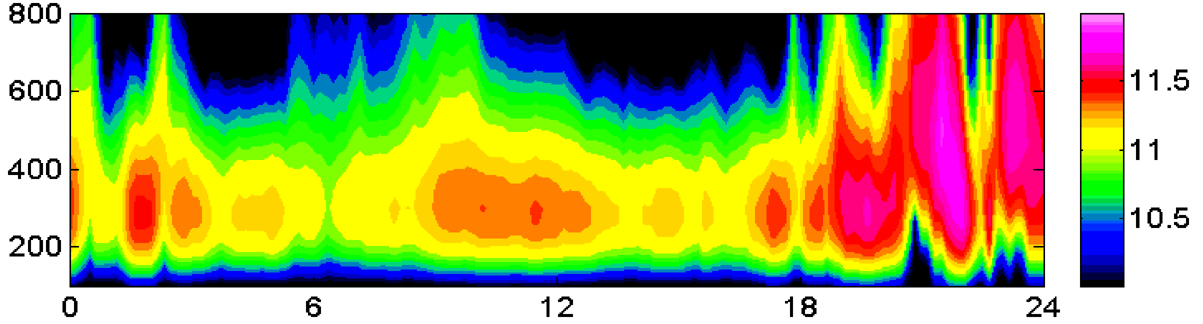

Tomography propagated across the polar cap

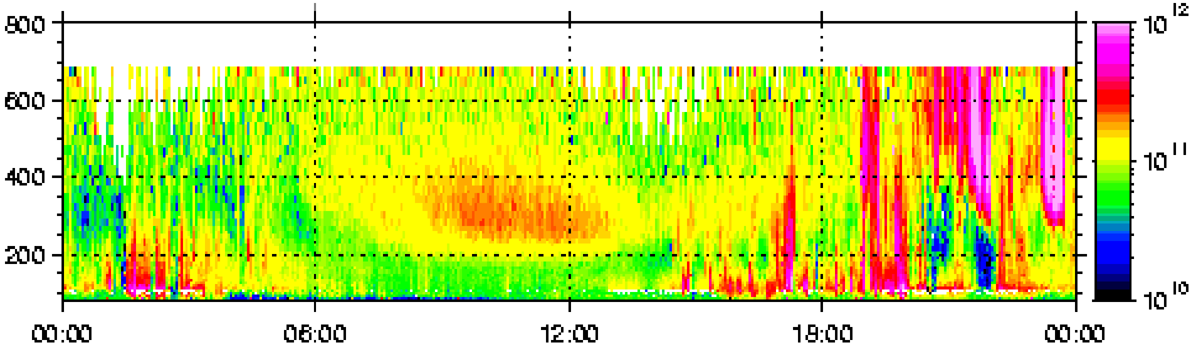

EISCAT radar in Scandinavia

Mitchell et al., 2008, doi:10.1029/181GM09.

Polar tongue of ionisation during storms

- Neutral winds can push plasma along (up) the field lines, to where the plasma recombination rate is slower.
- ExB drift may have a vertical component at mid-latitudes.
- Other mechanisms (e.g., chemical or compositional changes) could be more important during storm recovery phases.

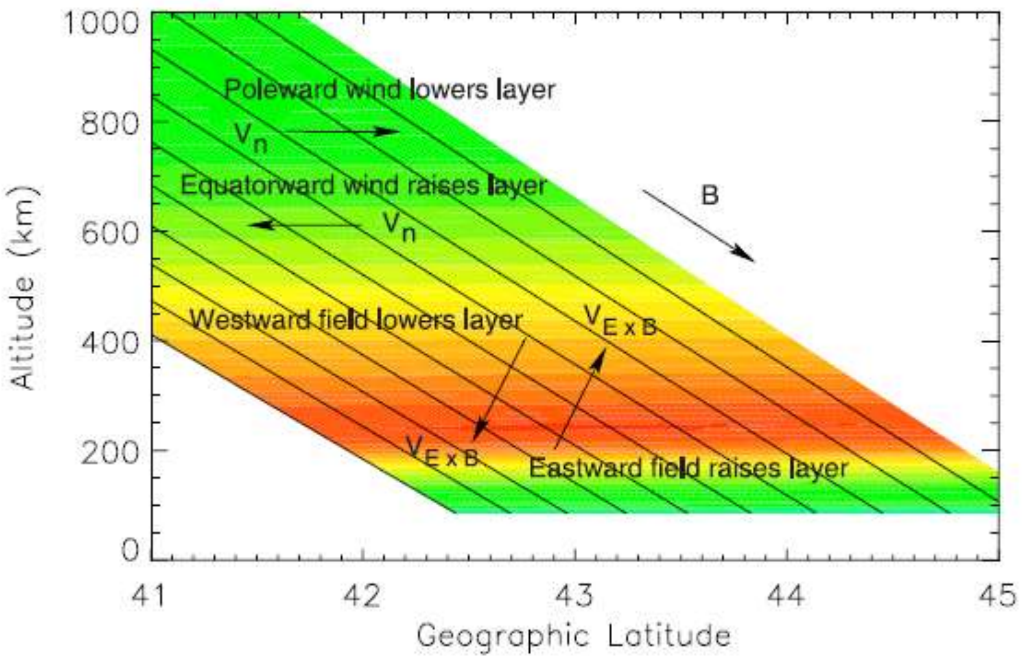

Swisdak et al., 2006, doi:10.1029/2005GL024973

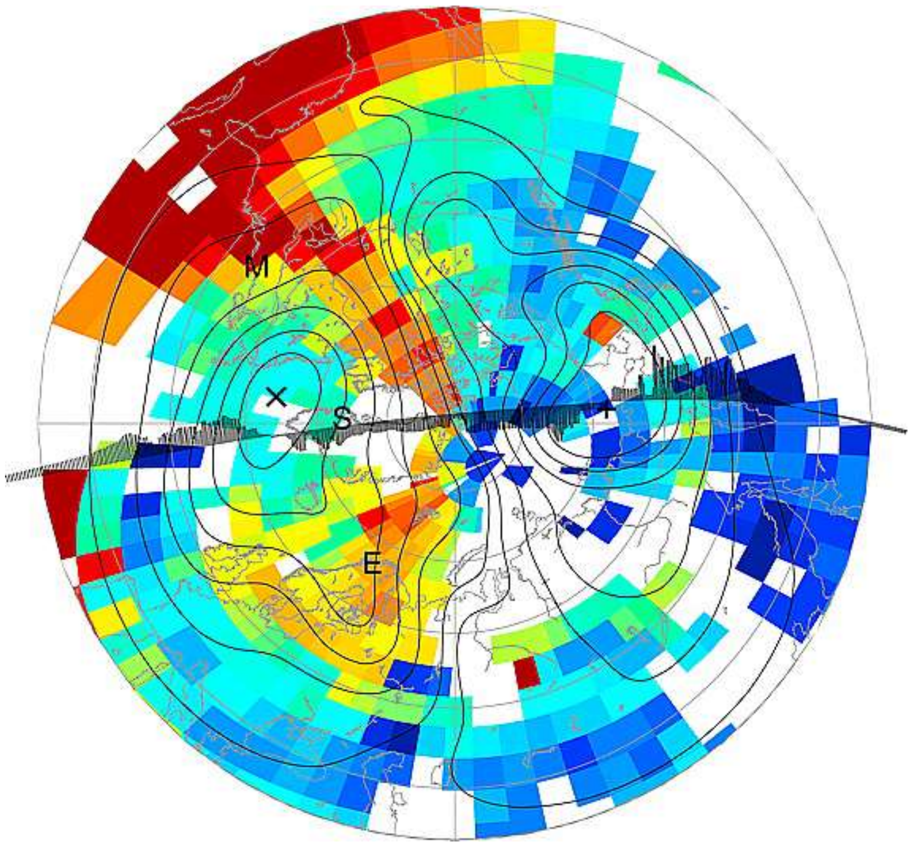

Foster et al., 2005, doi:10.1029/2004JA010928

Example: 20-Nov-2003 geomagnetic (super)storm

- The storm is isolated with a quiet pre-storm day (19-Nov).
- Formation of the high-latitude anomaly is expected during the main phase (12 - 21UT).
- The tongue would be forming in North American sector (dayside during the main phase) spreading anti-sunward.
- More on the 20-Nov-2003 superstorm:
  - Foster et al., 2005, doi:10.1029/2004JA010928
  - Pokhotelov et al., 2008, doi:10.1029/2008JA013109
  - Pokhotelov et al., 2021, doi:10.5194/angeo-39-833-2021

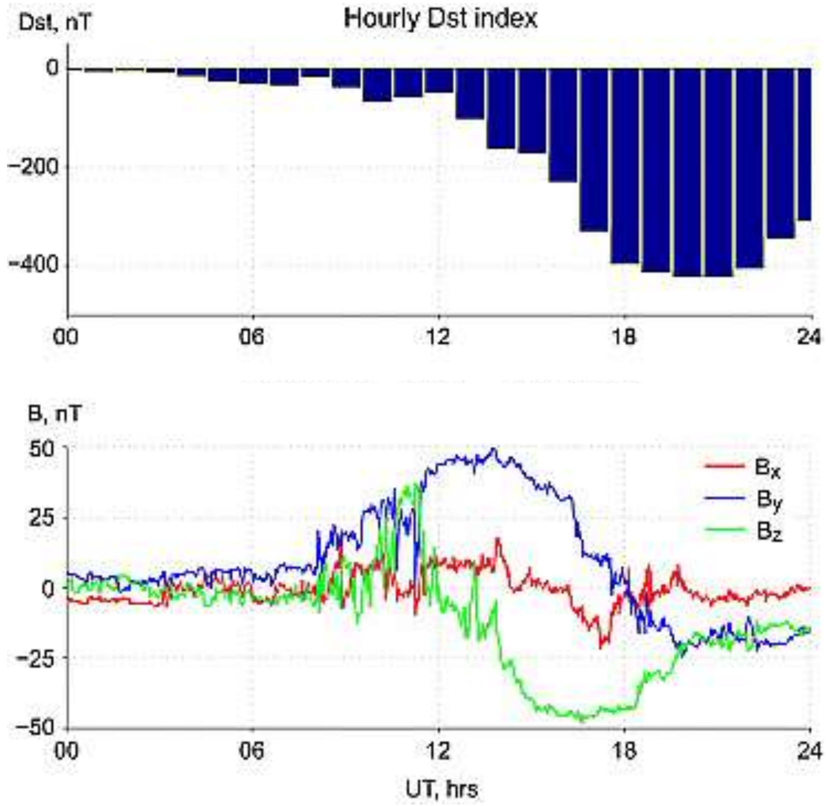

Pokhotelov et al., 2008
doi:10.1029/2008JA013109

TIE-GCM Simulations: polar cap view

- TIE-GCM simulation of the TOI with Weimer model.
- Animated polar projections (above 30°N).
- TOI maximises over North American Atlantic sector during the main phase (16-18 UT).
- At 18-20 UT large amounts of transported plasma reach over the polar cap into Scandinavian sector.

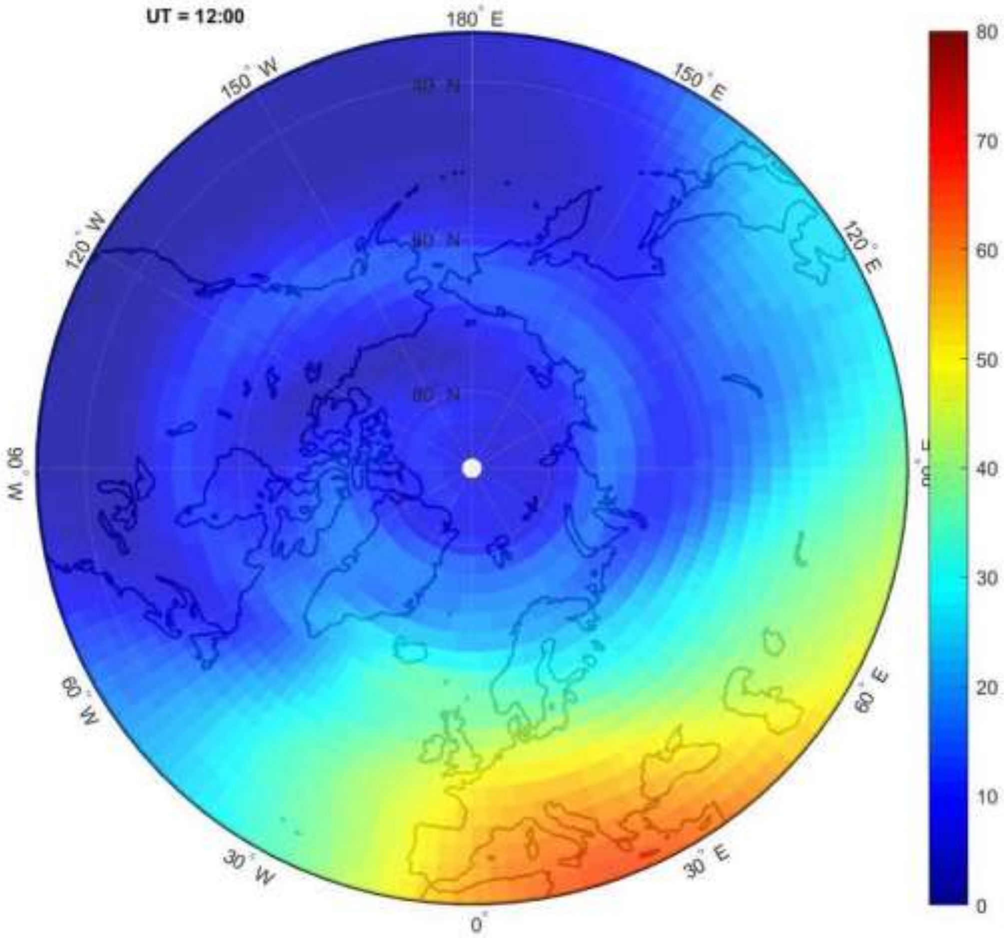

TEC and simulated ionospheric heights from TIEGCM

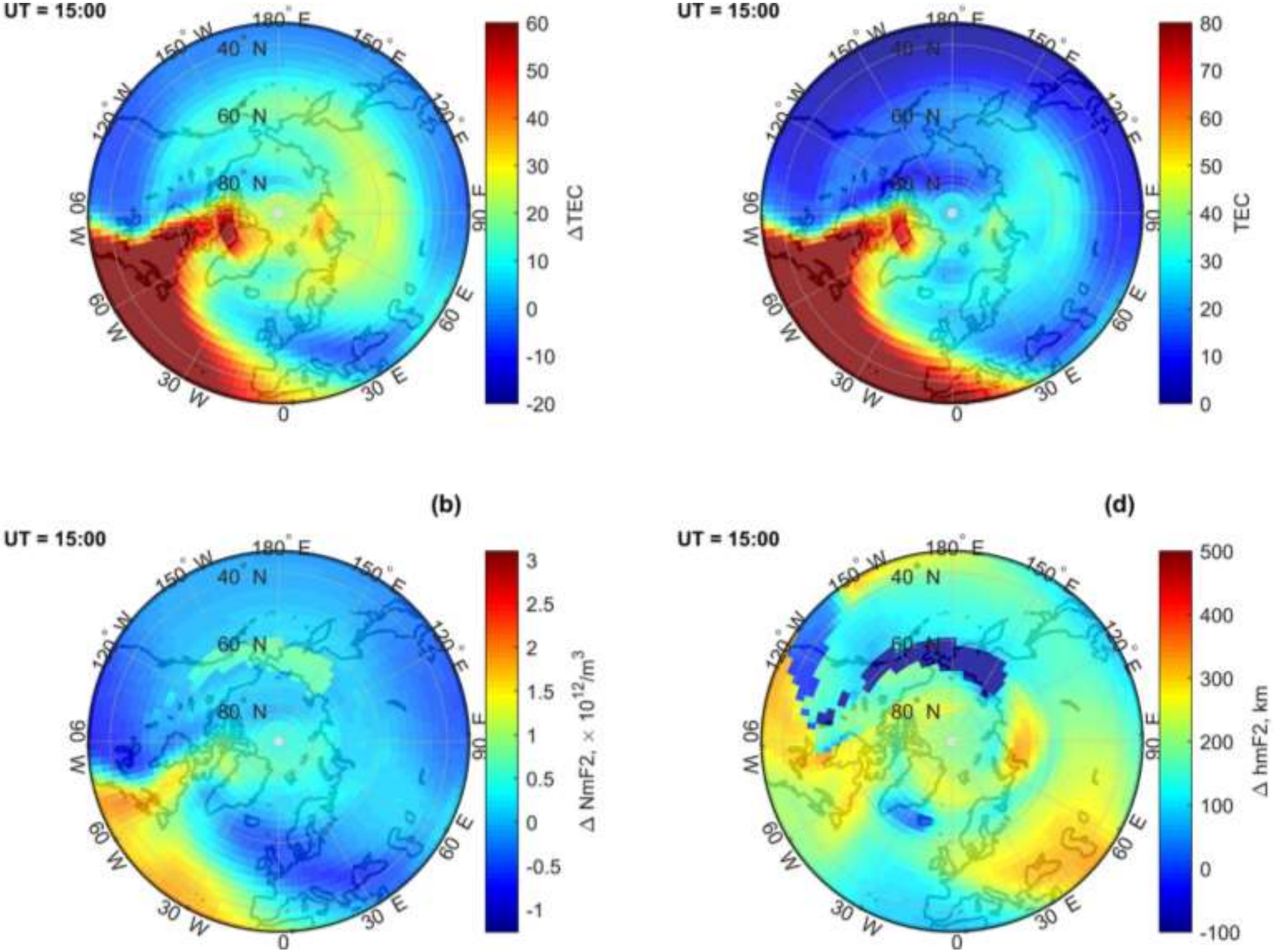

Pokhotelov et al., 2021
doi:10.5194/angeo-39-833-2021

DLR

TEC and simulated ionospheric heights from TIEGCM

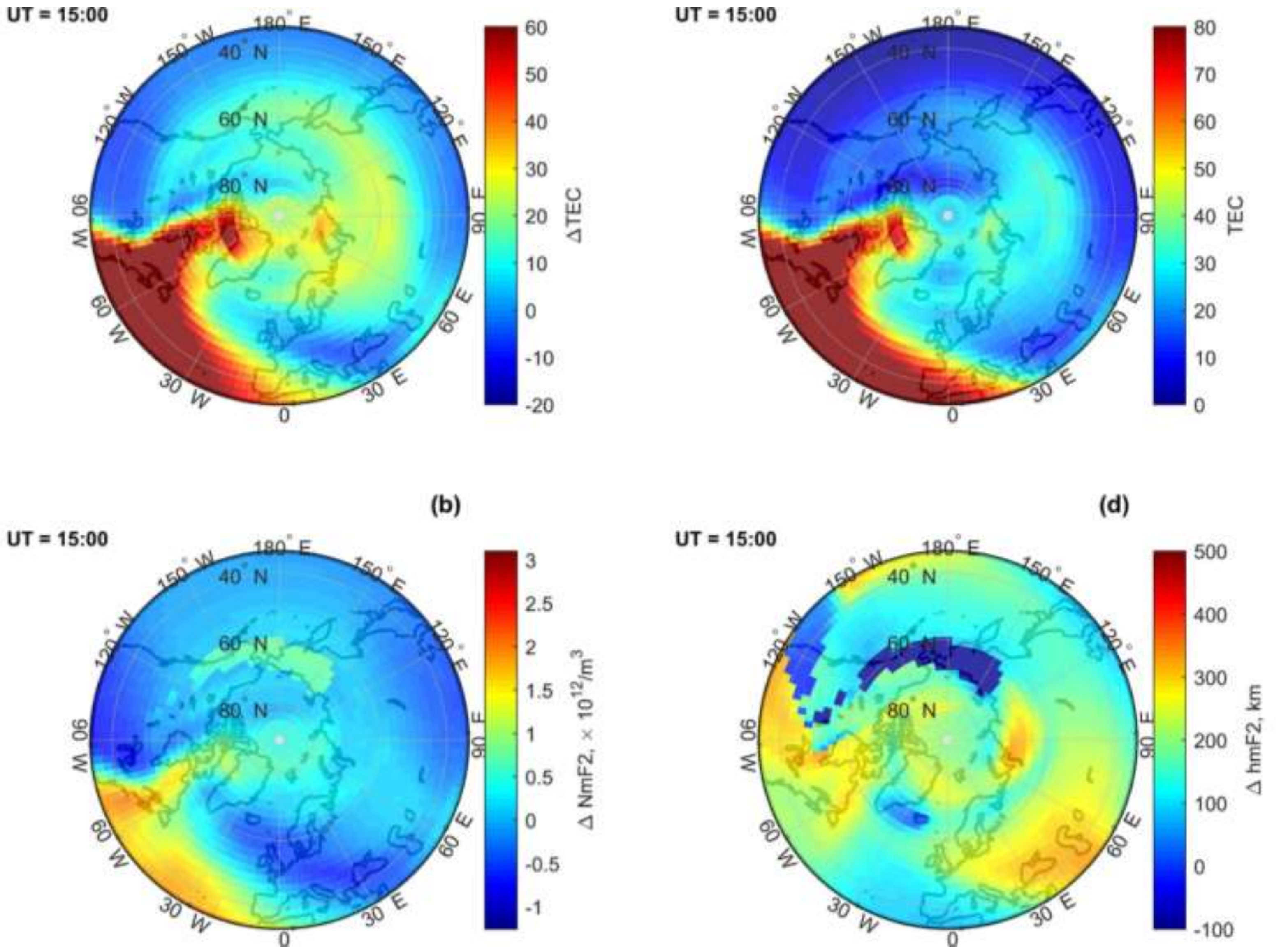

Pokhotelov et al., 2021
doi:10.5194/angeo-39-833-2021

Comparison to the simulations of different geomagnetic storms

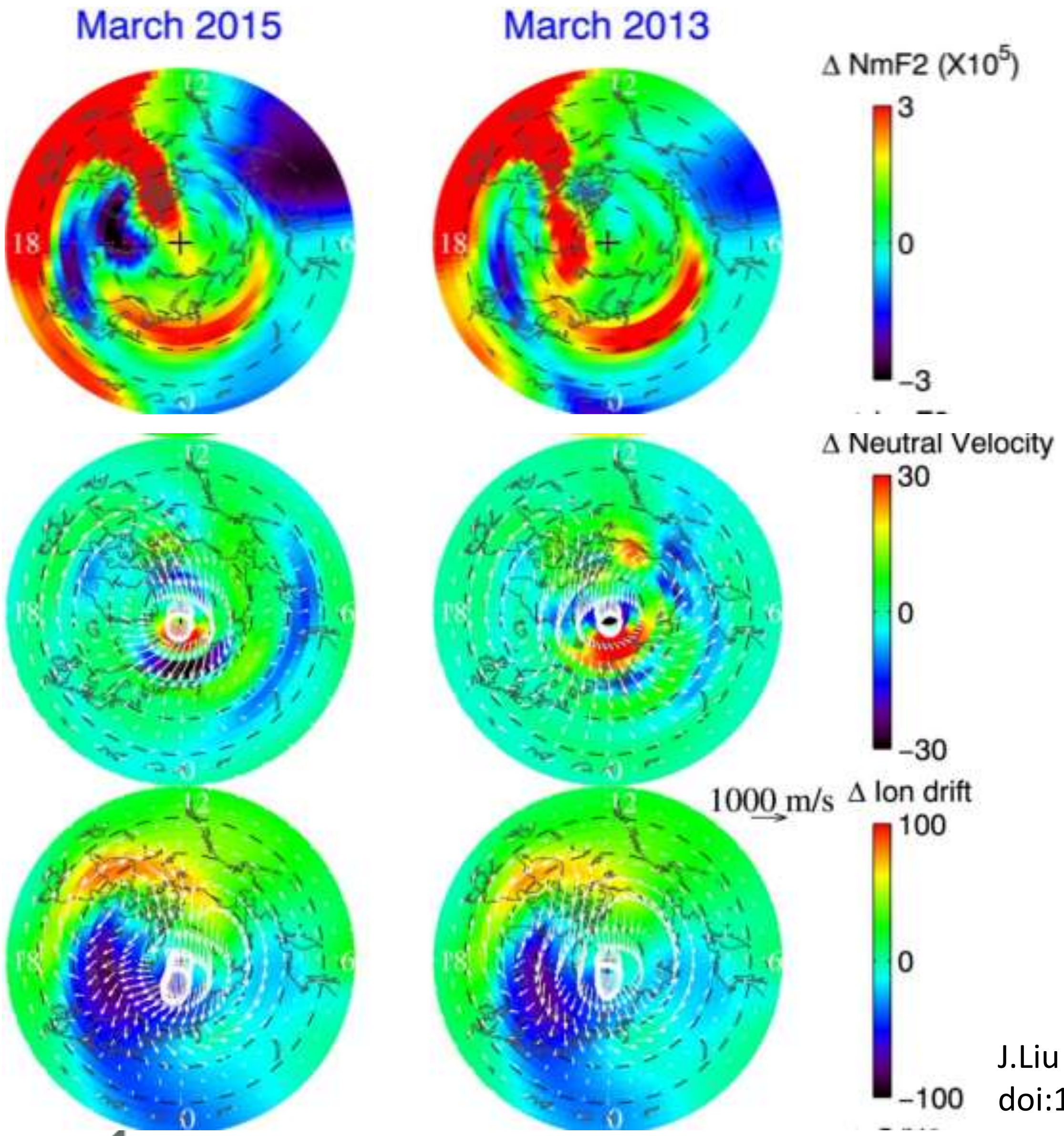

- J.Liu et al., JGR, 2016, doi:10.1002/2016JA022882
- TIE-GCM simulation of the TOI with Weimer ExB transport model for Mar 2015 (left) and Mar 2013 (right) storms.
- Geomagnetic storms of different origins:
  - CIR- and HSS-driven storms: Pokhotelov et al., 2009; 2010 doi:10.1029/2009JA014216, doi:10.1098/rspa.2010.0080
  - CME-driven storms, with the focus on neutral dynamics/chemistry: Klimenko et al., 2019, doi:10.1029/2018SW002143

J.Liu et al., JGR, 2016
doi:10.1002/2016JA022882

Frictional heating theory, models and measurements

$$T_i = T_n + \frac{m_n}{3k}(u_i - u_n)^2 = T_n + \frac{25}{3} \cdot 10^{-4} \cdot (u_i - u_n)^2$$

$$\frac{m_n}{3kB^2} = 0.33 \cdot 10^6$$

$T_n; u_n$: model neutral atmosphere

at 300 km

u_i: EISCAT

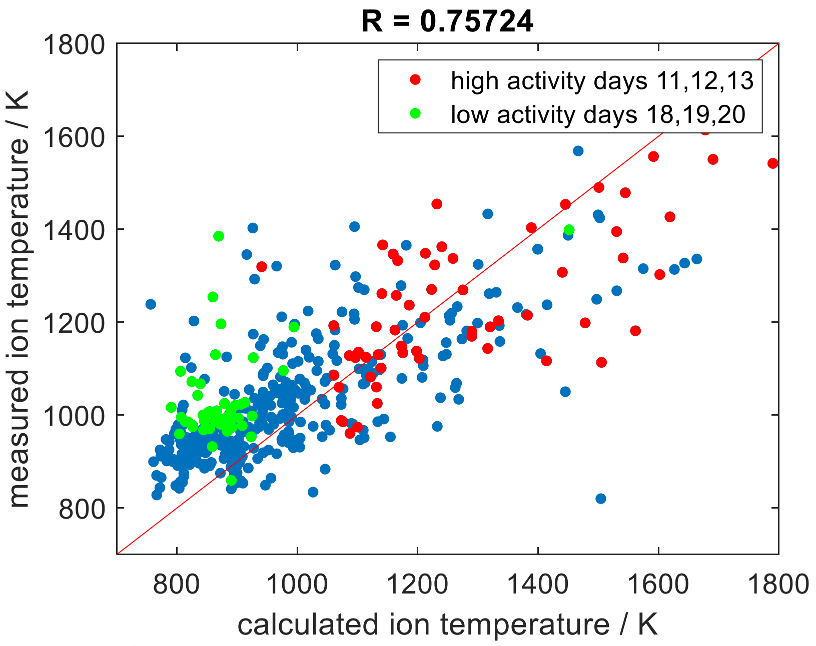

u_i: WACCM-X SD

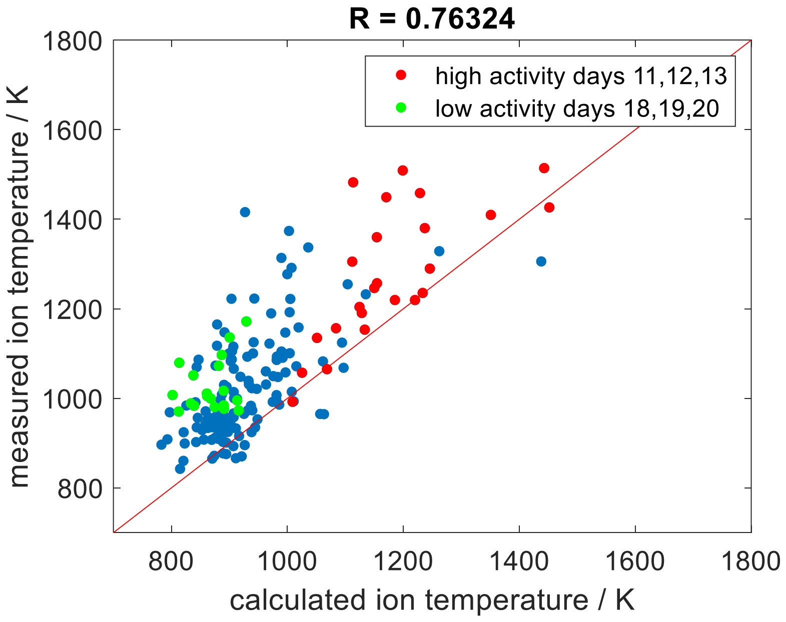

u_i: TIE-GCM

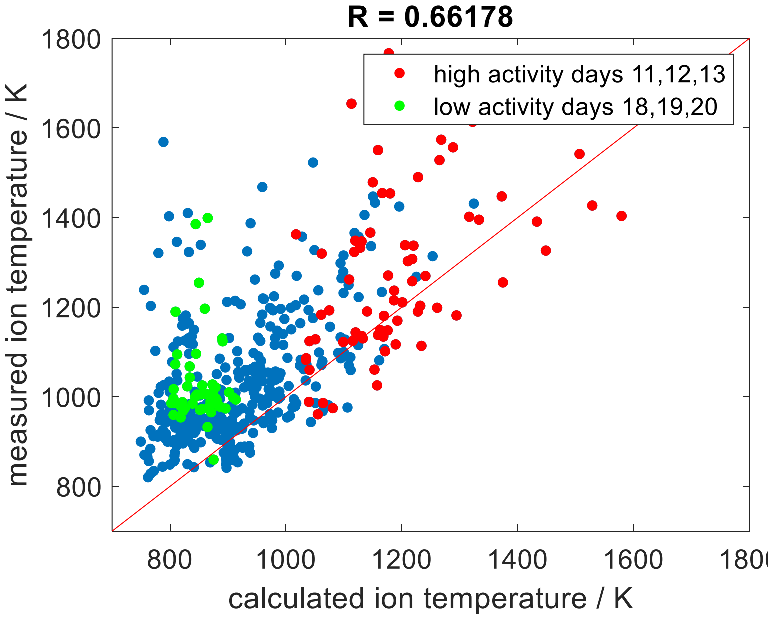

Selected references

- Günzkofer et al., JGR, 2022 https://doi.org/10.1002/essoar.10511116.1 (pre-print)
- Pokhotelov et al., Ann. Geophys., 2021 https://doi.org/10.5194/angeo-39-833-2021
- Klimenko et al., Space Weather, 2019 https://doi.org/10.1029/2018SW002143
- Liu, J., et al., JGR, 2016, https://doi.org/10.1002/2016JA022882
- Pokhotelov et al., JGR, 2009 https://doi.org/10.1029/2009JA014216
- Pokhotelov et al., JGR 2008 https://doi.org/10.1029/2008JA013109
- Mitchell et al., AGU Geophys. Monograph 181, 2008, https://doi.org/10.1029/181GM09
- Swisdak et al., GRL, 2006, https://doi.org/10.1029/2005GL024973
- Foster et al, JGR, 2005, https://doi.org/10.1029/2004JA010928